THE JOURNAL OF PHYSICAL CHEMISTRY C

Article

Cite This: J. Phys. Chem. C 2018, 122, 23191−23199

pubs.acs.org/JPCC

Grain Boundary Plays a Key Role in Carbon Diffusion in Carbon Irons Revealed by a ReaxFF Study

Kuan Lu,[†,‡,§] Chun-Fang Huo,[*,‡] Yurong He,[†,‡,§] Junqing Yin,[†,‡,§] Jinjia Liu,[†,‡,§] Qing Peng,[*,∥] Wen-Ping Guo,[‡] Yong Yang,[†,‡] Yong-Wang Li,[†,‡] and Xiao-Dong Wen[*,†,‡]

[†]State Key Laboratory of Coal Conversion, Institute of Coal Chemistry, Chinese Academy of Sciences, Taiyuan, Shanxi 030001, P. R. China

[‡]National Energy Center for Coal to Clean Fuels, Synfuels China Co., Ltd., Huairou District, Beijing 101400, P. R. China

[§]University of Chinese Academy of Sciences, No. 19A Yuquan Road, Beijing 100049, P. R. China

[∥]Nuclear Engineering and Radiological Sciences, University of Michigan, Ann Arbor, Michigan 48109, United States

Supporting Information

ABSTRACT: Carbon diffusion is a critical process to the manufacture of many industry products, such as iron carbides, stainless steels, and carbon materials. Here we investigate carbon diffusion induced by tensile, screw dislocation, edge dislocation, and polycrystal boundary through reactive molecular dynamics simulations with ReaxFF potentials. The temperature enhances the dynamics and therefore the carbon diffusion. The pre-existing defects promote the carbon diffusion with a linear relationship between carbon diffusion barrier and strain as well as line defect concentrations. Furthermore, we also observed a linear relationship between the carbon diffusion barrier and the volume fractions of the polycrystalline boundary, indicating that the grain boundary mechanism is prominent in carbon diffusion in the carbon iron.

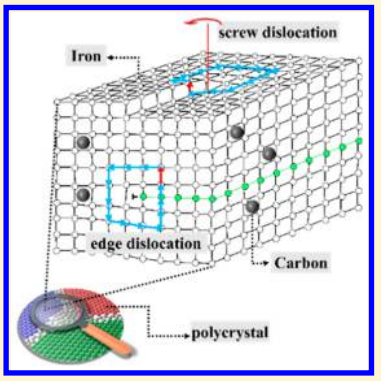

1. INTRODUCTION

The interactions between Fe and C atoms and ions play a pivotal role in the applications of iron in various industries, such as the iron and steel industry, Fischer−Tropsch industry, and the production of carbon material. For the iron and steel industry, the iron carbides,[1−4] formed by the carbonization of iron, are in general the main component of steels with an important impact on the structure, properties, and performance of steels. Specially, Fang et al.[2] demonstrated that the presence of Fe_3C in the steels is owing to its stability at the elevated temperature, which is also the origin of the predominance of Fe_3C to the lattice vibration and anomalous Curie−Weiss magnetic ordering. The metal dusting[5,6] is another critical case for Fe−C interaction due to its ability to degrade the strength of materials. For the Fischer−Tropsch industry, the iron carbides, such as Fe_3C[7−9] and Fe_5C_2,[10−13] are generally treated as the active phases, which first result from a phase transformation of iron phases involving α-Fe_2O_3 → Fe_3O_4 → FeO → α-Fe[14] and then are carbonized by the CO[15] or syngas.[16] However, because of overcarbonization of iron or the deposition of carbon on the iron surfaces, the catalyst easily becomes inactive as carbon materials including graphene[17] and carbon nanotube[18−20] will be also produced by the catalyst of iron carbides as well as iron.

Among all the above processes, mass transportation of carbon via diffusion in the iron plays a crucial role. Many researchers have investigated these processes through the experimental and theoretical methods. Experimental results[21−23] show that the activation energy of carbon Fickian diffusion in iron bulk is about 0.81−0.87 eV, the same as the predictions from the first-principles[24] and molecular dynamics (MD).[25−27] The activation energy is up to 1.87 eV[28,29] for carbon diffusion in Fe_3C. It is worth mentioning that most theoretical models studied are perfect crystal models without defects. On the contrary, experimental samples in general contain lots of defects, such as line defects including edge dislocations[30,31] and screw dislocations[30−32] and two-dimensional defects including grain boundaries[31,33] between polycrystals. These defects have a critical effect on the physical, mechanical, and chemical performance[34,35] of materials, especially the diffusion.[36,37] The grain boundaries[38] may act as efficient sinks for the excess interstitials and vacancies produced under irradiation. Carbons can diffuse to the dislocations forming a Cottrell atmosphere,[39] leading to the loss in metal plasticity and the increase in strength. In addition, the deformed grains can cause the local strain, resulting in the reduction of their stored energy by removing or rearranging the defects in the crystal structure.

Despite the importance, to what extent these defects and its concentration affect the carbon diffusion is still unknown. The

Received: August 7, 2018
Revised: September 13, 2018
Published: September 13, 2018

DOI: 10.1021/acs.jpcc.8b07650
J. Phys. Chem. C 2018, 122, 23191−23199

reasons can be attributed to two aspects. One is the limitation of experimental approaches. Traditional transmission electron microscopy (TEM) as the frequently used recognition technology of dislocation in materials represents a two-dimensional projection of a three-dimensional (3D) object which only provides limited information about 3D dislocations. The process occurring on time scales is too short to capture using *in situ* TEM. X-ray topography can image the 3D dislocation, but its resolution is reduced.[40] The other reason is the constraint from theoretical modeling. Only a few theoretical methods can be used to investigate carbon diffusion in the iron that is capable to model the effect of defects at the same time. The unique nature of carbon diffusion resulting from the defects existing in the real physical and catalysis process is still an active research subject. Among extensive models, the embedded atom method (EAM) improved by Margarita[41] and the modified embedded atom method (MEAM) modified by Byeong-Joo Lee[42] may be the best choices to study the carbon diffusion due to its distinguished merit to simulate the physical performance of metal, including the effect of defects. However, it is only suitable to the low carbon concentration situation owing to the lack of the accurate carbon−carbon interactions. In additional, it is incapable to deal with the chemical reactions. From the point of view of chemical reactions, the reactive force field (ReaxFF) is a good choice. ReaxFF advocated by van Duin and co-workers[43] was originally used to deal with the chemical reactions, with the capability to handle the mechanical behavior such as fracture. It had been validated by the implications of other materials.[44−47] Our previous work[27] had fitted the Fe−C parameters (RPOIC-2017) for the ReaxFF which could excellently describe the thermodynamical and dynamical behavior of carbon in bulk, different surfaces, and the subsurface.

In this study, we employ the Fe−C parameters (RPOIC-2017) to simulate the mechanical failure of bulk α-Fe and compare with the results of EAM and MEAM potential functions to assess its performance and optimal simulation parameters. We then adopt the selected parameters to execute the ReaxFF molecular dynamics (RMD) simulating the effect of tensile strain and defects, including screw dislocation, edge dislocation, and boundary of polycrystal, on carbon diffusion.

2. COMPUTATIONAL METHODS

2.1. EAM. The embedded atom method (EAM), derived by Baskes et al.,[48,49] is a pairwise form of interatomic potential which is especially suitable for metals. The energy is calculated by the following form:

$$E = \frac{1}{2}\sum_{i,j} V(ij) + \sum_{i} F(\overline{\rho}_i)$$
$$\overline{\rho}_i = \sum_{i} \rho(r_{i,j}) \quad (1)$$

where $V(ij)$ is the interatomic potential, r_{ij} represents the distance between atom i and atom j, and F is the embedding energy as a function of atom i surrounded by electron density $\overline{\rho}_i$.

2.2. MEAM. The modified embedded-atom method (MEAM) potential proposed by Baskes[50] is an extension of the EAM to include angular forces. The total energy of a system is same with the EAM. But different from the EAM, the MEAM has angular terms, which make it suitable for modeling metal and alloys as well as covalently bonded materials. The details of MEAM potential functions are supplied in the Supporting Information.

2.3. ReaxFF. ReaxFF is an empirical force field based on the concept of bond order[43] which is the function of bond length and bond energy, and it allows for bond to break and form in a dynamic simulation. The general form of ReaxFF energy[51] is

$$E_{\text{systerm}} = E_{\text{bond}} + E_{\text{lp}} + E_{\text{over}} + E_{\text{under}} + E_{\text{val}} + E_{\text{tors}} + E_{\text{C2}} + E_{\text{tripl}} + E_{\text{conj}} + E_{\text{H-bond}} + E_{\text{vdw}} + E_{\text{Coulomb}} \quad (2)$$

One of the most important features of ReaxFF is the use of electronegativity equilibration method (EEM)[52] with shielding to calculate the charge distribution updated every iteration during the RMD simulation that determines the geometry of material and further affects the total potential energy of material. The bond orders calculation also updates every iteration which firmly establishes the bonded interaction; the nonbonded interaction is comprised of Coulomb and van der Waals interaction which are calculated between every pair of atoms.

All MD simulations were performed by LAMMPS,[53] and the structures were identified by the OVITO.[54] All the atomic structures in our model were initially optimized through conjugate gradient method to athermal structures, followed by canonical ensemble (NVT) under the temperature T = 300 K for 100 ps to reached thermodynamics equilibrium. These well-equilibrated configurations are then subjected to further study. The simulations employed the velocity-Verlet integrator.

3. RESULTS AND DISCUSSION

3.1. Mechanical Fracture. We have previously reported that RPOIC-2017 potential is good in describing the carbon diffusion in α-Fe in addition to the chemical reactions, opposed to MEAM.[27] In this study, we focus on the mechanical properties. To assess the ability of RPOIC-2017 in predicting physical performance, we conducted the mechanical fracture simulation of bulk α-Fe by external press to emulate its stress−strain curves. We examined the effect of different sizes of box as well as the effect of different force fields including MEAM and EAM. The setup of the tensile model (Figure 1) consists of three parts. The first part is the fixed zone in which all atoms are fixed. The second part is the active zone in which the atoms are free to move according to the interaction potential. The last one is the mobile zone which is used as the "handle" to apply the stress. During the tensile process, the two ends are assumed to maintain the perfect lattice. The lattice constant of bcc iron is 2.84 Å.

Five systems were examined including 20 × 6 × 6 (1440 atoms), 20 × 10 × 10 (4000 atoms), 20 × 14 × 14 (7840 atoms), 20 × 16 × 16 (10240 atoms), and 20 × 18 × 18 (12960 atoms). Periodic boundary conditions are applied in the Z direction (out of plane in Figure 1), opposed to the free surfaces in other two dimensions. For MEAM and EAM, the time step of 1 fs and the strain of 100 Å/fs were used and the time step of 0.5 fs and strain of 0.001 Å/fs for ReaxFF. The Fe−C interaction parameters of MEAM, EAM, and ReaxFF were fitted by Laalitha et al.,[55] Mendelev et al.,[56] and Kuan Lu et al.,[27] respectively. Figure 2a shows that with an increase of system size the effect of system size is decreasing. The samller

DOI: 10.1021/acs.jpcc.8b07650
J. Phys. Chem. C 2018, 122, 23191−23199

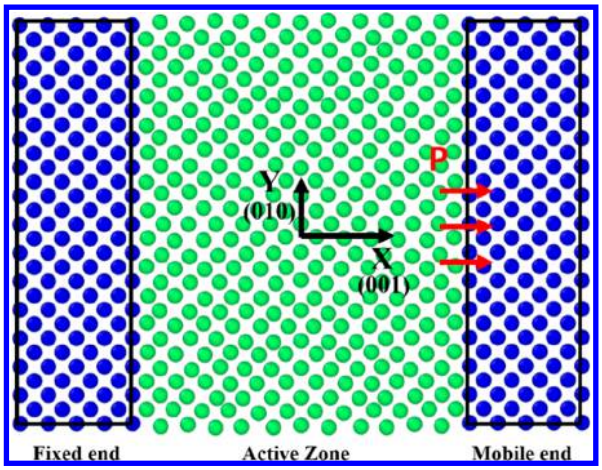

Figure 1. Tensile model of bulk α-Fe whose structure is the body-centered cubic (BCC). All the atoms are iron atom. Green atoms present the active zone, and blue atoms stand for the boundary area.

systems of 20 × 6 × 6 and 20 × 10 × 10 cannot correctly simulate the iron stress−strain curves. When the system size increases to 20 × 14 × 14, it can provide a converged description, which reproduces well the elastic deformation, plastic deformation, and fracture without much computational burden simultaneously. Therefore, we choose the 20 × 14 × 14 system for all the following simulations. When the strain ε_x < 5%, the MEAM, EAM, and ReaxFF predict a similar stress−strain behavior (Figure 2b). Its corresponding yield strength is 9.2, 6.5, and 7.7 GPa, respectively, and its line relationship between stress σ and strain ε_x is $\sigma = 155.9\varepsilon_x$,$\sigma = 171.1\varepsilon_x$, and $\sigma = 155.6\varepsilon_x$, respectively.

In addition, the Young's modulus is very close to the experimental value 131.73 GPa,[57] the theoretical analyses value 154 GPa,[58] and the numerical result of EAM 142.3 GPa.[59] When the strain ε_x > 5%, the irreversible damages are produced in the system, and the system has the plastic deformation. It is well-known that there is a strain hardening region before the failure of iron.[60] Three potentials predict different trends in stress−strain behavior. The MEAM gives a bad result without strain hardening, which is not suitable to describe the mechanical fracture of iron. The EAM and ReaxFF present a well consistency in strain hardening, indicating the capability in modeling fracture of iron. The percentage elongation is between 0.2 and 0.3, close to the empirical value 0.3−0.5 and the reference value about 0.4[58,61] when the fracture occurs. The fracture stress is 11.3 and 11.7 GPa, respectively, consistent with the reference value 8.4−13.5 GPa.[58] All those results indicate that the RPOIC-2017 can regenerate the physical performance of α-Fe well.

3.2. Effect of Strain on the Carbon Diffusion.

3.2.1. Fickian Diffusion. We first investigated the Fickian diffusion of carbon in iron without globally applied strain field. We used a model of bulk α-Fe with 16000 iron atoms and 80 carbon atoms randomly distributed in the simulation box. The initial edge length is 5.68 nm, 5.68 nm, and 5.68 nm for a three-dimensional periodical box. A time step of 0.25 fs was adopted. The diffusion coefficient of carbon was obtained by calculating the mean-square displacements (MSD) of carbon atoms when the system is under thermodynamics equilibrium. We used Einstein's relation for the MSD and obtained the corresponding diffusion coefficients (shown in the Supporting Information). In the absence of strain, carbon atoms move randomly in all three directions (Figure 3a) presented by a similar trend in any single direction of MSD. The displacement of carbon atoms shows an increasing trend near 1 order of magnitude with the temperature increasing.

3.2.2. Uniaxial Tensile-Induced Diffusion. The structures were stretched along the x direction (along the ⟨001⟩ direction) on account of the observation of carbon diffusion under the stress. The strain rate of 0.001 Å/fs was applied, which is equivalent to 100 m/s. The strain of structures was 5%, 8%, 10%, and 12%. The elastic limit is 12%. From the Figure 3b, we can see that although the tensile direction is the x direction, the MSD's in the three individual directions are nearly the same, which indicates that the carbon atoms diffuse isotropically in three directions. Similar results are observed in other tensile cases (Figure 3c). The difference existed in the increased amplitude of MSD with the increasing of temperature, which implies that strain-induced deformation of structures not only promotes the carbon diffusion, but also its degree of deformation relates to the carbon diffusion.

3.2.3. Diffusion Barrier. The Arrhenius plots had been fitted to the diffusion coefficient with and without strain (Figure 4a) to obtain the diffusion barrier. When the strains are 0% and 12%, respectively; its corresponding diffusion barriers are 0.63 and 0.44 eV. The result of Fickian diffusion is very close to the experimental and reference value.[21−23] The applied strain

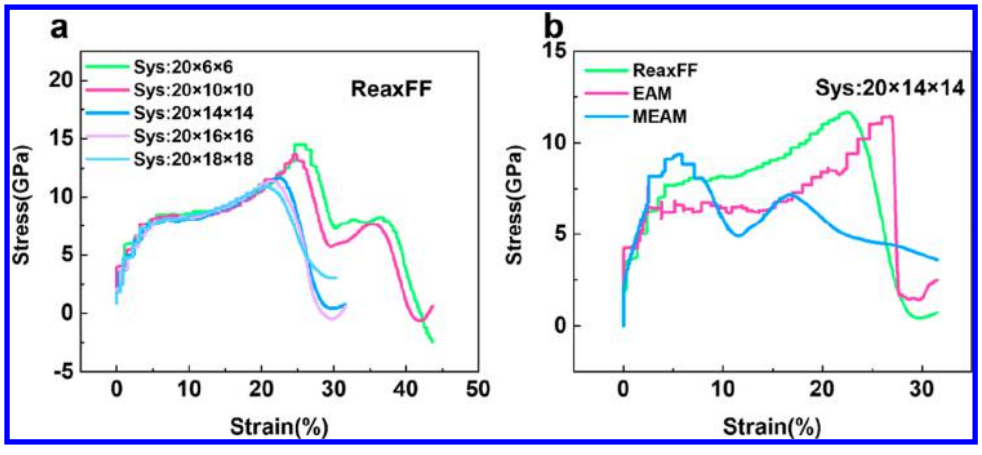

Figure 2. (a) Mechanical fracture with different simulation parameters for MEAM, EAM, and ReaxFF potential functions. Benchmark of different system size for ReaxFF. (b) Comparison for different force field.

DOI: 10.1021/acs.jpcc.8b07650
J. Phys. Chem. C 2018, 122, 23191−23199

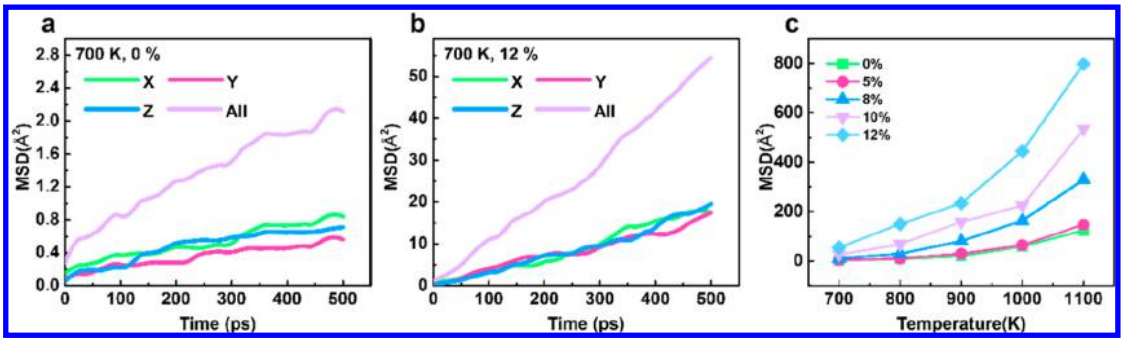

Figure 3. (a) MSD for the Fickian diffusion without strain at 700 K. (b) MSD for the Fickian diffusion with the maximum strain at 700 K. (c) MSD under different strains and different temperatures.

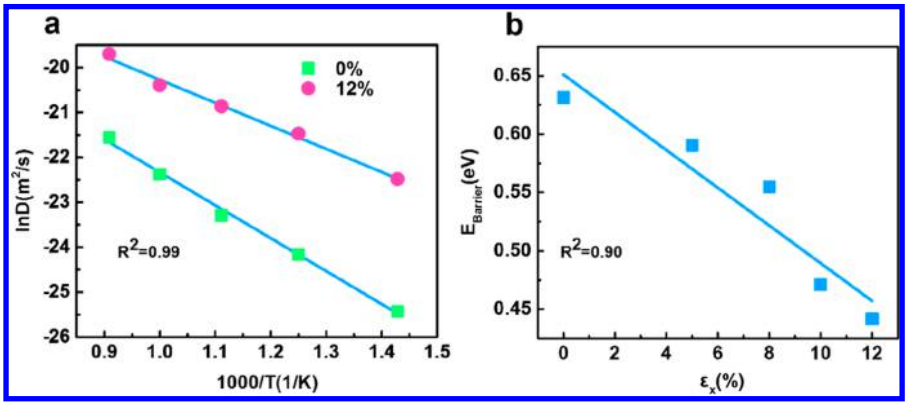

Figure 4. (a) Linear relationship between the carbon diffusion coefficients and the temperature. (b) Linear relationship between the strains and the carbon diffusion barrier.

monotonically reduces the diffusion barrier of carbon. We fitted the relationship between strain (ε_x) and the carbon diffusion barrier ($E_{barrier}$). We obtain a linear relationship (Figure 4b): $E_{barrier} = -1.61\varepsilon_x + 0.65$ without constraints. Once we set the intercept of equation to experimental value, we obtained the carbon diffusion barrier energy as a function of uniaxial strain along the x direction: $E_{barrier} = -1.61\varepsilon_x + 0.87$. With this relationship, we can speculate the chemical barrier of carbon diffusion from the physical strain. We might conclude that strain accelerates the diffusion carbon and the formation of carbides.

3.2.4. Evolution of Structure. A few snapshots of the atomic configurations during the process of mechanical fracture calculated by ReaxFF are shown in Figure 5. We employed common neighbor analysis (CNA) embedded in the OVITO to analyze the phase transformation quantitatively. This technique identifies the local structure in atomic systems by using information about the mutual relation between neighbors. The structure of pure iron experiences a transformation from body-centered cubic (BCC) to face-centered cubic (FCC). At the same time, the crystal parameter is increased. When the strain is relatively small, such as 5%, the FCC structure occurs occupying the all normalized active zone structures about 3%. With the increase of strain to 8%, the percent of FCC increases suddenly to 38.5%, which implies that the bulk iron had generated the irreversible damage. When the strain increases to 12%, about 50.5% FCC structures are observed. We also observed an apparent necking in the y direction. The change of structure may be the main reason for increasing of carbon diffusion coefficient, and it also may be the main reason that the different structure carbide formed, such as the Fe_4C formed from the FCC structure.

3.3. Effect of Dislocations on the Carbon Diffusion. In bcc metals, owing to the lower mobility of $1/2a\langle 111\rangle$ screw dislocations than edge dislocation, it is believed to control the low-temperature plastic deformation. The plasticity becomes complex when the defects are introduced. On the one hand, the activation energy of dislocation movement could be influenced by the presence of defects in the crystal, such as the interstitial carbon. On the other hand, the dislocation movement, such as the reduction of dislocation by recovery, causes a change of defect concentration which has a vital effect on the carbon diffusion. We designed our study to shed a light on the effect of defects on the carbon diffusion. We adopted a box of 5.74 nm × 5.74 nm × 5.74 nm which is composed of 19710 iron atoms for edge dislocation and a box of 7.03 nm × 6.09 nm × 4.97 nm which is composed of 18000 iron atoms for screw dislocation. Here we considered the edge dislocations with Burgers vectors $1/2[111]$, slip plane normal $[\bar{1}\ 10]$, and dislocation line direction $[\bar{1}\ \bar{1}\ 2]$. By a similar method, the screw dislocations $1/2\langle 111\rangle\{\bar{1}\ 10\}$ were created. The defects were randomly distributed. Along the dislocation line, it was the only direction where periodic boundary conditions (PBC) have been used. All atoms of the system were allowed to relax except those in the outside layer of none PBC directions about one atom thick. The atom in the outsider layer were fixed. All defect models (Figure 6) in this paper were created by Atomsk.[62]

Figure 7a shows a linear relationship between carbon diffusion barrier and screw dislocation concentrations, as $E_{barrier} = -0.027N_s + 0.62$, where N_s represents the numbers of

DOI: 10.1021/acs.jpcc.8b07650
J. Phys. Chem. C 2018, 122, 23191−23199

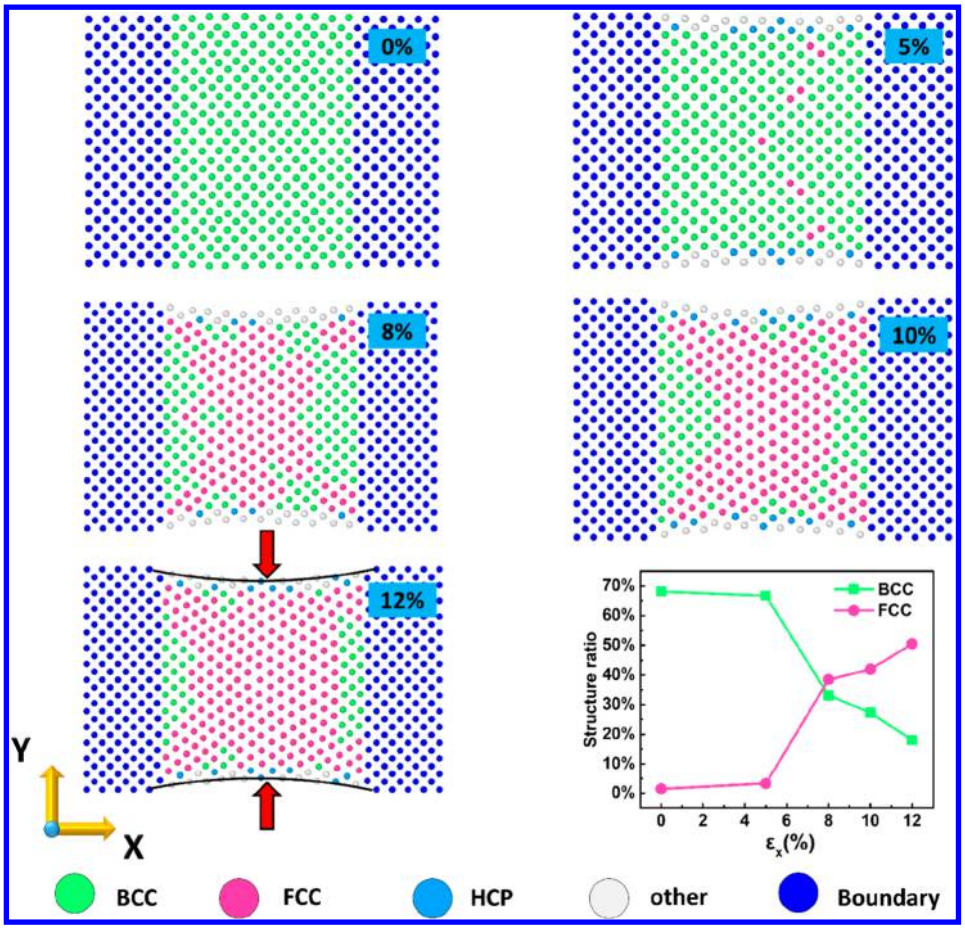

Figure 5. Different structures for α-Fe are presented by different colors. The blue shows the BCC, the green expresses the face-centered cubic (FCC), and the red indicates the hexagonal close-packed (HCP). The white stands for the other structures, and the blue area in the two ends means the "handle".

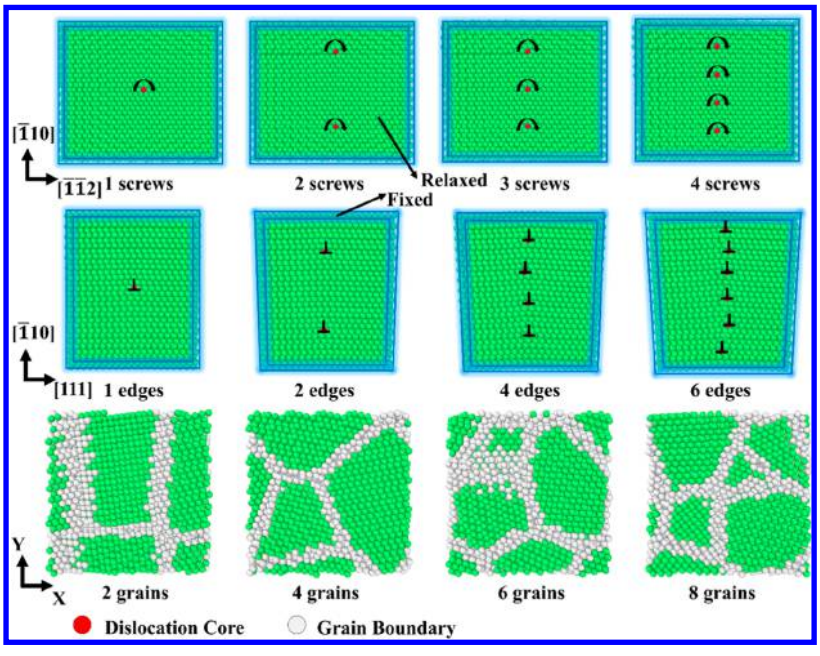

Figure 6. Models of different defects for α-Fe: top row for screw dislocation; middle row for edge dislocations; bottom row for grain boundaries between polycrystals.

screws in crystal. This linear relationship indicates that screw concentrations have a substantial effect on the carbon diffusion barrier in the metallic recovery process. At the same time, it may have induced a change of material performance. Similarly,

DOI: 10.1021/acs.jpcc.8b07650
J. Phys. Chem. C 2018, 122, 23191−23199

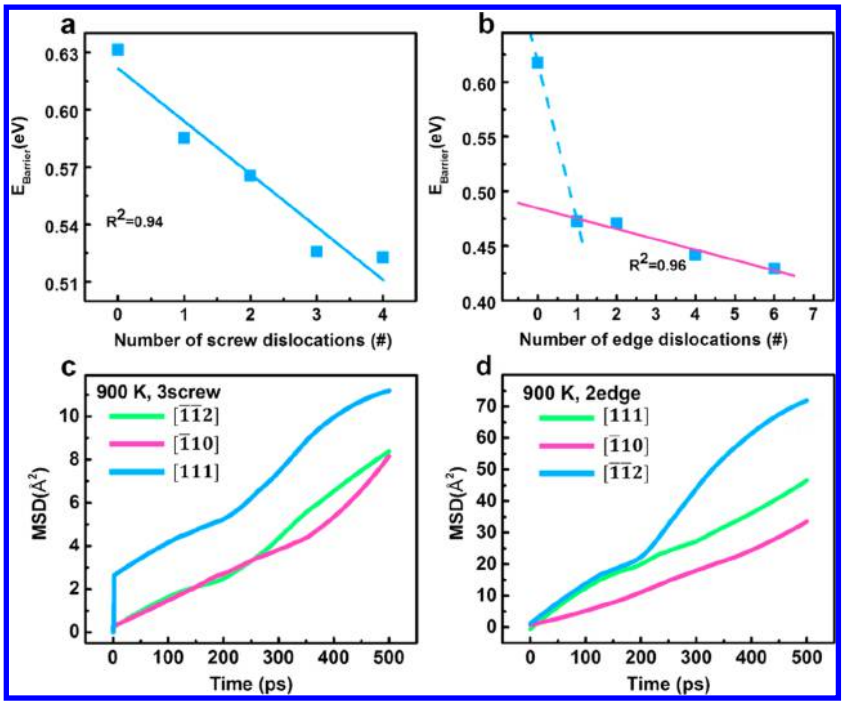

Figure 7. (a) Linear relationship between the defect concentrations and the carbon diffusion barrier under screw dislocation. (b) Linear relationship between the defect concentrations and the carbon diffusion barrier under edge dislocation. The dashed line is only guide for the eyes. (c) MSD of different directions in the defected models under screw dislocation. (d) MSD of different directions in the defected models under edge dislocation.

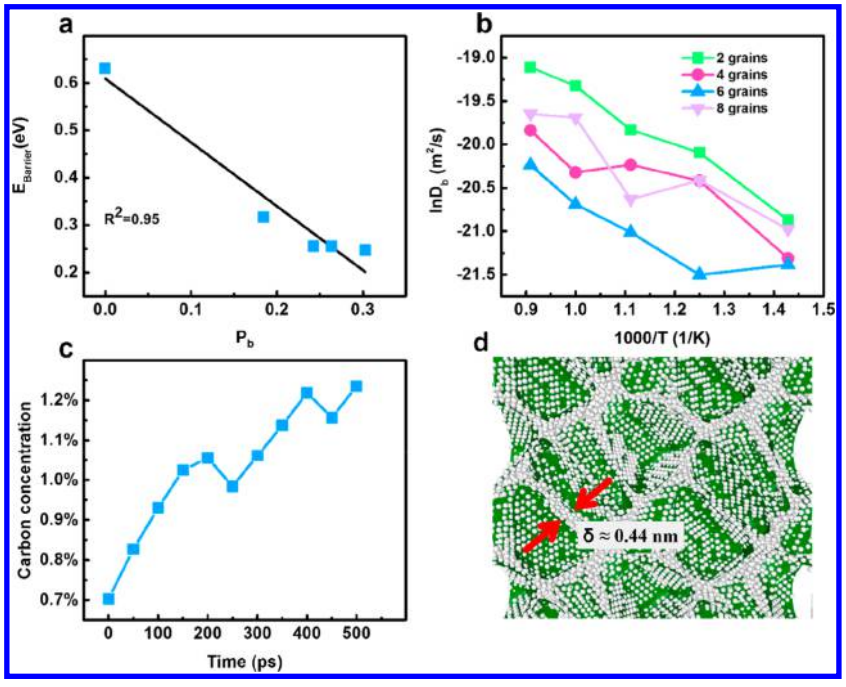

Figure 8. (a) Linear relationship between the volume fraction of boundary and the carbon diffusion barrier. (b) Linear relationship between the natural logarithms of the carbon intrinsic diffusion coefficient in the boundary and the reciprocal of temperature. (c) Increasing carbon fraction in the boundary. (d) Snapshot of grain boundary indicating the GB width delta. Atom color scheme: iron atom (white); surface of grain boundary (green).

a linear relationship is observed in Figure 7b: $E_{barrier} = -0.0095N_e + 0.48$, where N_e represents the numbers of edges in crystal. The occurrence of edge dislocations can obviously reduce the carbon diffusion barrier. The concentration of the edge dislocations also affects the carbon diffusion barrier. Furthermore, the carbon diffusion is mainly along the no-defect direction in the defected models, as shown in Figure 7c,d.

3.4. Effect of Grain Boundary on the Carbon Diffusion. Polycrystal irons are much more common than single crystal iron. The grain boundary (GB) between polycrystals can trap the interstitial atoms. It commonly

DOI: 10.1021/acs.jpcc.8b07650
J. Phys. Chem. C 2018, 122, 23191−23199

believed that grain boundary is responsible for the embrittlement or occasionally enhancement of material strength. However, its influence on the carbon diffusion is still unknown. Herein, we studied the effect of polycrystal on the carbon diffusion barrier. We adopted the box of 5.47 nm × 6.09 nm × 7.03 nm with three-dimensional periodic boundary conditions (PBC) which is composed of 15992 iron atoms. It contains 2, 4, 6, and 8 grains with random crystallographic orientations constructing by the Voronoi construction method. The average grain size in the box is 2.7, 2.0, 1.8, and 1.6 nm with about 0.44 nm boundary width (Figure 8d), and its distribution can be found in Figure 6. All atoms in the box are allowed to relax. A linear relationship is shown in Figure 8a: $E_{barrier} = -1.35P_b + 0.609$, where P_b represents the ratio of boundary volume to the total volume. Inspired by the Harrison's classification[63] and the average gain size being also small, we adopted the equation $D_{eff} = P_bD_b + (1 - P_b)D$ to calculate the intrinsical diffusion coefficient of carbon in the boundary, where D_{eff} is the carbon diffusion coefficient in polycrystals, D is the carbon diffusion coefficient in a perfect system, and D_b is the carbon diffusion coefficient in the boundary. We then found that ln D_b has a relationship with the reciprocal of temperature for all the polycrystals with a similar slope (Figure 8b), and we obtained an average diffusion barrier of about 0.22 eV, which may be the intrinsical diffusion barrier of carbon in the polycrystals. This is related to that the atom density is lower in the boundary region than that in the bulk, which may provide more space for carbon to move, resulting in a smaller diffusion barrier.

Figure 8c shows that GB carbon concentration, which is the ratio of carbon atoms located in the grain boundary to the total number of atoms located in the grain boundary, is increasing with the elapse of time, indicating that the boundary has more free volume than the perfect system and can capture carbon atoms, which means that the boundary also has a critical effect on the carbon diffusion barrier. Owing to the random direction of individual grain, the MSD of individual direction of the models is not able to characterize the diffusion around grain boundary; only the total MSD is meaningful. Compared with the effect of strain and line dislocations, the absolute value of slope of boundary is the maximum, and it indicates that the boundary may be the most influential factor to carbon diffusion.

4. CONCLUSIONS

We first assessed the performance of three different interatomic potentials (EAM, MEAM, and RPOIC-2017) of iron and carbon by simulating the mechanical fracture using molecular dynamics simulations. We confirmed that ReaxFF in form of the RPOIC-2017 can be used to explore the physical performance of iron. Second, we examined the strain effect on the carbon diffusion. The results show that strain-induced structure transformation can effectively and monotonically reduce the carbon diffusion barrier and promote the carbon diffusion coefficient. The temperature can also strikingly promote the carbon diffusion. A linear relationship is observed between the carbon diffusion barrier and strain. It is critical not only to understand the diffusion process and carbonization of iron but also to speculate the chemical diffusion barrier from the physical strain. Third, we considered the effect of defects, including the screw dislocations, edge dislocations, and polycrystal boundary on the carbon diffusion. The results show that the existence of defects can prominently improve the carbon diffusion coefficient and a linear relationship exists between the carbon diffusion barrier and defects concentrations or the volume fractions of grain boundary. The grain boundary of polycrystals may be the main factor to affect the carbon diffusion barrier.

■ ASSOCIATED CONTENT

Supporting Information

The Supporting Information is available free of charge on the ACS Publications website at DOI: 10.1021/acs.jpcc.8b07650.

Description of the MEAM potential function with the calculation of MSD and barrier (PDF)

■ AUTHOR INFORMATION

Corresponding Authors

*(X.-D.W.) E-mail wxd@sxicc.ac.cn.
*(C.-F.H.) E-mail huochunfang@synfuelschina.com.cn.
*(Q.P.) E-mail qpeng@umich.edu.

ORCID

Xiao-Dong Wen: 0000-0001-5626-8581

Notes

The authors declare no competing financial interest.

■ ACKNOWLEDGMENTS

The authors are grateful the financial support from the National Natural Science Foundation of China (Nos. 21473229, 91545121, 21603252, 21703274, 21703272, and 21273261), Shanxi Province Science Foundation for Youth (No. 201601D021048), and Chinese Academy of Science and Synfuels CHINA. Co., Ltd. We also acknowledge the innovation foundation of Institute of Coal Chemistry, Chinese Academy of Sciences, Hundred-Talent Program of Chinese Academy of Science, Shanxi Hundred-Talent Program, and National Thousand Young Talents Program of China.

■ REFERENCES

(1) Hirotsu, Y.; Nagakura, S. Crystal Structure and Morphology of the Carbide Precipitated from Martensitic High Carbon Steel During the First Stage of Tempering. *Acta Metall.* **1972**, *20*, 645−655.

(2) Fang, C. M.; Sluiter, M. H. F.; van Huis, M. A.; Ande, C. K.; Zandbergen, H. W. Origin of Predominance of Cementite among Iron Carbides in Steel at Elevated Temperature. *Phys. Rev. Lett.* **2010**, *105*, 055503.

(3) Jack, K. H.; Wild, S. Nature of χ-Carbide and Its Possible Occurrence in Steels. *Nature* **1966**, *212*, 248−250.

(4) Ernst, F.; Cao, Y.; Michal, G. M. Carbides in Low-Temperature-Carburized Stainless Steels. *Acta Mater.* **2004**, *52*, 1469−1477.

(5) Grabke, H. J.; Müller-Lorenz, E. M.; Schneider, A. Carburization and Metal Dusting on Iron. *ISIJ. Int.* **2001**, *41*, S1−S8.

(6) Young, D.; Zhang, J. Metal Dusting: Catastrophic Corrosion by Carbon. *JOM* **2012**, *64*, 1461−1469.

(7) Le Caer, G.; Dubois, J. M.; Pijolat, M.; Perrichon, V.; Bussiere, P. Characterization by Moessbauer Spectroscopy of Iron Carbides Formed by Fischer−Tropsch Synthesis. *J. Phys. Chem.* **1982**, *86*, 4799−4808.

(8) Liao, X.-Y.; Cao, D.-B.; Wang, S.-G.; Ma, Z.-Y.; Li, Y.-W.; Wang, J.; Jiao, H. Density Functional Theory Study of CO Adsorption on the (100), (001) and (010) Surfaces of Fe_3C. *J. Mol. Catal. A: Chem.* **2007**, *269*, 169−178.

(9) Deng, L.-J.; Huo, C.-F.; Liu, X.-W.; Zhao, X.-H.; Li, Y.-W.; Wang, J.; Jiao, H. Density Functional Theory Study on Surface Cxhy Formation from CO Activation on $Fe_3C(100)$. *J. Phys. Chem. C* **2010**, *114*, 21585−21592.

DOI: 10.1021/acs.jpcc.8b07650
J. Phys. Chem. C 2018, 122, 23191−23199

(10) Cao, D.-B.; Li, Y.-W.; Wang, J.; Jiao, H. Adsorption and Reaction of Surface Carbon Species on $Fe_5C_2(001)$. *J. Phys. Chem. C* **2008**, *112*, 14883−14890.
(11) Petersen, M. A.; van den Berg, J.-A.; van Rensburg, W. J. Role of Step Sites and Surface Vacancies in the Adsorption and Activation of CO on χ-Fe_5C_2 Surfaces. *J. Phys. Chem. C* **2010**, *114*, 7863−7879.
(12) Cao, D.-B.; Li, Y.-W.; Wang, J.; Jiao, H. Chain Growth Mechanism of Fischer−Tropsch Synthesis on $Fe_5C_2(001)$. *J. Mol. Catal. A: Chem.* **2011**, *346*, 55−69.
(13) Yang, C.; Zhao, H.; Hou, Y.; Ma, D. Fe_5C_2 Nanoparticles: A Facile Bromide-Induced Synthesis and as an Active Phase for Fischer−Tropsch Synthesis. *J. Am. Chem. Soc.* **2012**, *134*, 15814−21.
(14) Ding, M.; Yang, Y.; Wu, B.; Li, Y.; Wang, T.; Ma, L. Study on Reduction and Carburization Behaviors of Iron Phases for Iron-Based Fischer−Tropsch Synthesis Catalyst. *Appl. Energy* **2015**, *160*, 982−989.
(15) Janbroers, S.; Crozier, P. A.; Zandbergen, H. W.; Kooyman, P. J. A Model Study on the Carburization Process of Iron-Based Fischer−Tropsch Catalysts Using in situ TEM−EELS. *Appl. Catal., B* **2011**, *102*, 521−527.
(16) de Smit, E.; Cinquini, F.; Beale, A. M.; Safonova, O. V.; van Beek, W.; Sautet, P.; Weckhuysen, B. M. Stability and Reactivity of η-χ-θ Iron Carbide Catalyst Phases in Fischer−Tropsch Synthesis: Controlling μC. *J. Am. Chem. Soc.* **2010**, *132*, 14928−14941.
(17) Awadallah, A. E.; Aboul-Enein, A. A.; Kandil, U. F.; Taha, M. R. Facile and Large-Scale Synthesis of High Quality Few-Layered Graphene Nano-Platelets Via Methane Decomposition over Unsupported Iron Family Catalysts. *Mater. Chem. Phys.* **2017**, *191*, 75−85.
(18) Nishimura, K.; Okazaki, N.; Pan, L.; Nakayama, Y. In Situ Study of Iron Catalysts for Carbon Nanotube Growth Using X-Ray Diffraction Analysis. *Jpn. J. Appl. Phys.* **2004**, *43*, L471.
(19) Oshima, H.; Shimazu, T.; Siry, M.; Mibu, K. Analysis of Fe Catalyst During Carbon Nanotube Synthesis by Mossbauer Spectroscopy. *J. Phys. Chem. C* **2009**, *113*, 18523−18526.
(20) He, Z.; Maurice, J.-L.; Gohier, A.; Lee, C. S.; Pribat, D.; Cojocaru, C. S. Iron Catalysts for the Growth of Carbon Nanofibers Fe, Fe_3C or Both. *Chem. Mater.* **2011**, *23*, 5379−5387.
(21) da Silva, J. R. G.; McLellan, R. B. Diffusion of Carbon and Nitrogen in B.C.C. Iron. *Mater. Sci. Eng.* **1976**, *26*, 83−87.
(22) Wert, C. A. Diffusion Coefficient of C in A-Iron. *Phys. Rev.* **1950**, *79*, 601−605.
(23) McLellan, R. B.; Wasz, M. L. Carbon Diffusivity in B.C.C. Iron. *J. Phys. Chem. Solids* **1993**, *54*, 583−586.
(24) Jiang, D. E.; Carter, E. A. Carbon Dissolution and Diffusion in Ferrite and Austenite from First Principles. *Phys. Rev. B: Condens. Matter Mater. Phys.* **2003**, *67*, 214103.
(25) Becquart, C. S.; Raulot, J. M.; Bencteux, G.; Domain, C.; Perez, M.; Garruchet, S.; Nguyen, H. Atomistic Modeling of an Fe System with a Small Concentration of C. *Comput. Mater. Sci.* **2007**, *40*, 119−129.
(26) Tapasa, K.; Barashev, A. V.; Bacon, D. J.; Osetsky, Y. N. Computer Simulation of Carbon Diffusion and Vacancy−Carbon Interaction in A-Iron. *Acta Mater.* **2007**, *55*, 1−11.
(27) Lu, K.; Huo, C. F.; Guo, W. P.; Liu, X. W.; Zhou, Y.; Peng, Q.; Yang, Y.; Li, Y. W.; Wen, X. D. Development of a Reactive Force Field for the Fe-C Interaction to Investigate the Carburization of Iron. *Phys. Chem. Chem. Phys.* **2018**, *20*, 775−783.
(28) Schneider, A.; Inden, G. Carbon Diffusion in Cementite (Fe_3C) and Hägg Carbide (Fe_5C_2). *CALPHAD: Comput. Coupling Phase Diagrams Thermochem.* **2007**, *31*, 141−147.
(29) Levchenko, E.; Evteev, A.; Belova, I.; Murch, G. Molecular Dynamics Simulation and Theoretical Analysis of Carbon Diffusion in Cementite. *Acta Mater.* **2009**, *57*, 846−853.
(30) Hosseini Nasab, F.; Hossein Nedjad, S.; Karimi, S. A Comparison between the Dislocation Structure of Ball-Milled Iron and Copper as Derived from the X-Ray Diffraction Peak Profile Analyses. *Phys. Met. Metallogr.* **2013**, *114*, 1069−1073.
(31) Chen, C. C.; Zhu, C.; White, E. R.; Chiu, C. Y.; Scott, M. C.; Regan, B. C.; Marks, L. D.; Huang, Y.; Miao, J. Three-Dimensional Imaging of Dislocations in a Nanoparticle at Atomic Resolution. *Nature* **2013**, *496*, 74−7.
(32) Forouzanmehr, N.; Nili-Ahmadabadi, M.; Bönisch, M. The Analysis of Severely Deformed Pure Fe Structure Aided by X-Ray Diffraction Profile. *Phys. Met. Metallogr.* **2016**, *117*, 624−633.
(33) Suzuki, Y.; Mori, A.; Fujiwara, T.; Tamura, K. Precise Characterization of Grain Structures, Stacking Disorders, and Lattice Disorders of a Close-Packed Colloidal Crystal. *J. Cryst. Growth* **2011**, *322*, 109−113.
(34) Sutton, A.; Balluff, R. *Interfaces in Crystalline Materials*; Oxford Science Publications: New York, 1995.
(35) Wu, Z.; Curtin, W. A. The Origins of High Hardening and Low Ductility in Magnesium. *Nature* **2015**, *526*, 62−67.
(36) Veiga, R. G. A.; Perez, M.; Becquart, C. S.; Domain, C.; Garruchet, S. Effect of the Stress Field of an Edge Dislocation on Carbon Diffusion In α-Iron: Coupling Molecular Statics and Atomistic Kinetic Monte Carlo. *Phys. Rev. B: Condens. Matter Mater. Phys.* **2010**, *82*, 054301.
(37) Clouet, E.; Garruchet, S.; Nguyen, H.; Perez, M.; Becquart, C. S. Dislocation Interaction with C in α-Fe: A Comparison between Atomic Simulations and Elasticity Theory. *Acta Mater.* **2008**, *56*, 3450−3460.
(38) Vetterick, G. A.; Gruber, J.; Suri, P. K.; Baldwin, J. K.; Kirk, M. A.; Baldo, P.; Wang, Y. Q.; Misra, A.; Tucker, G. J.; Taheri, M. L. Achieving Radiation Tolerance through Non-Equilibrium Grain Boundary Structures. *Sci. Rep.* **2017**, *7*, 12275.
(39) Cottrell, A. H.; Bilby, B. A. Dislocation Theory of Yielding and Strain Ageing of Iron. *Proc. Phys. Soc., London, Sect. A* **1949**, *62*, 49.
(40) Ludwig, W.; Cloetens, P.; Hartwig, J.; Baruchel, J.; Hamelin, B.; Bastie, P. Three-Dimensional Imaging of Crystal Defects by 'Topo-Tomography'. *J. Appl. Crystallogr.* **2001**, *34*, 602−607.
(41) Ruda, M.; Farkas, D.; Garcia, G. Atomistic Simulations in the Fe−C System. *Comput. Mater. Sci.* **2009**, *45*, 550−560.
(42) Lee, B.-J. A Modified Embedded-Atom Method Interatomic Potential for the Fe−C System. *Acta Mater.* **2006**, *54*, 701−711.
(43) van Duin, A. C. T.; Dasgupta, S.; Lorant, F.; Goddard, W. A., III Reaxff: A Reactive Force Field for Hydrocarbons. *J. Phys. Chem. A* **2001**, *105*, 9396−9409.
(44) Koo, B.; Subramanian, N.; Chattopadhyay, A. Molecular Dynamics Study of Brittle Fracture in Epoxy-Based Thermoset Polymer. *Composites, Part B* **2016**, *95*, 433−439.
(45) Ostadhossein, A.; Kim, S.-Y.; Cubuk, E. D.; Qi, Y.; van Duin, A. C. T. Atomic Insight into the Lithium Storage and Diffusion Mechanism of SiO_2/Al_2O_3 Electrodes of Lithium Ion Batteries: Reaxff Reactive Force Field Modeling. *J. Phys. Chem. A* **2016**, *120*, 2114−2127.
(46) Penev, E. S.; Artyukhov, V. I.; Yakobson, B. I. Basic Structural Units in Carbon Fibers: Atomistic Models and Tensile Behavior. *Carbon* **2015**, *85*, 72−78.
(47) Zhang, C.; van Duin, A. C. T.; Seo, J. W.; Seveno, D. Weakening Effect of Nickel Catalyst Particles on the Mechanical Strength of the Carbon Nanotube/Carbon Fiber Junction. *Carbon* **2017**, *115*, 589−599.
(48) Daw, M. S.; Baskes, M. I. Embedded-Atom Method: Derivation and Application to Impurities, Surfaces, and Other Defects in Metals. *Phys. Rev. B: Condens. Matter Mater. Phys.* **1984**, *29*, 6443−6453.
(49) Daw, M. S.; Foiles, S. M.; Baskes, M. I. The Embedded-Atom Method: A Review of Theory and Applications. *Mater. Sci. Rep.* **1993**, *9*, 251−310.
(50) Baskes, M. I. Modified Embedded-Atom Potentials for Cubic Materials and Impurities. *Phys. Rev. B: Condens. Matter Mater. Phys.* **1992**, *46*, 2727−2742.
(51) Liu, L.; Jaramillo-Botero, A.; Goddard, W. A., III; Sun, H. Development of a Reaxff Reactive Force Field for Ettringite and Study of Its Mechanical Failure Modes from Reactive Dynamics Simulations. *J. Phys. Chem. A* **2012**, *116*, 3918−25.

DOI: 10.1021/acs.jpcc.8b07650
J. Phys. Chem. C 2018, 122, 23191−23199

(52) Rappe, A. K.; Goddard, W. A., III Charge Equilibration for Molecular Dynamics Simulations. *J. Phys. Chem.* **1991**, *95*, 3358−3363.
(53) Plimpton, S. Fast Parallel Algorithms for Short-Range Molecular Dynamics. *J. Comput. Phys.* **1995**, *117*, 1−19.
(54) Stukowski, A. Visualization and Analysis of Atomistic Simulation Data with Ovito−the Open Visualization Tool. *Modell. Simul. Mater. Sci. Eng.* **2010**, *18*, 015012.
(55) Liyanage, L. S. I.; Kim, S.-G.; Houze, J.; Kim, S.; Tschopp, M. A.; Baskes, M. I.; Horstemeyer, M. F. Structural, Elastic, and Thermal Properties of Cementite (Fe_3C) Calculated Using a Modified Embedded Atom Method. *Phys. Rev. B: Condens. Matter Mater. Phys.* **2014**, *89*, 094102.
(56) Mendelev, M. I.; Han, S.; Srolovitz, D. J.; Ackland, G. J.; Sun, D. Y.; Asta, M. Development of New Interatomic Potentials Appropriate for Crystalline and Liquid Iron. *Philos. Mag.* **2003**, *83*, 3977−3994.
(57) Adams, J. J.; Agosta, D. S.; Leisure, R. G.; Ledbetter, H. Elastic Constants of Monocrystal Iron from 3 to 500 K. *J. Appl. Phys.* **2006**, *100*, 113530.
(58) Hu, S. Y.; Ludwig, M.; Kizler, P.; Schmauder, S. Atomistic Simulations of Deformation and Fracture of A-Fe. *Modell. Simul. Mater. Sci. Eng.* **1998**, *6*, 567.
(59) Byggmästar, J.; Granberg, F.; Kuronen, A.; Nordlund, K.; Henriksson, K. O. E. Tensile Testing of Fe and Fecr Nanowires Using Molecular Dynamics Simulations. *J. Appl. Phys.* **2015**, *117*, 014313.
(60) Bhattacharyya, A.; Ravichandran, G.; Rittel, D. Strain Rate Effect on the Evolution of Deformation Texture for A-Fe. *Metall. Mater. Trans. A* **2006**, *37*, 1137−1145.
(61) Sandoval, L.; Urbassek, H. M. Solid-Solid Phase Transitions in Fe Nanowires Induced by Axial Strain. *Nanotechnology* **2009**, *20*, 325704.
(62) Hirel, P. Atomsk: A Tool for Manipulating and Converting Atomic Data Files. *Comput. Phys. Commun.* **2015**, *197*, 212−219.
(63) Mishin, Y.; Herzig, C. Grain Boundary Diffusion: Recent Progress and Future Research. *Mater. Sci. Eng., A* **1999**, *260*, 55−71.

DOI: 10.1021/acs.jpcc.8b07650
J. Phys. Chem. C 2018, 122, 23191−23199